

Supplementary material

Dialkylsulfate formation in sulfuric acid-seeded secondary organic aerosol produced using an outdoor chamber under natural sunlight

Jiaying Li,^A Myoseon Jang^{A,B} and Ross L. Beardsley^A

^ADepartment of Environmental Engineering Sciences, University of Florida, PO Box 116450, Gainesville, FL 32611, USA.

^BCorresponding author. Email: mjang@ufl.edu

Calibration of the C-RUV method for measuring $[H^+]$ in aerosol

In the present study, aerosol acidity was measured using colorimetry integrated with a reflectance UV-visible spectrometer (C-RUV),^[1,2] which is an optical technique and directly measures the proton concentration ($[H^+]$, mol L⁻¹) of the $NH_4^+-H^+-SO_4^{2-}-H_2O$ aerosol collected on the filter without heating or solvent extraction. Aerosols were collected on a 13-mm-diameter sampling filter (Gelman Science Palflex, TX40H120-WW) that was dyed with an indicator (0.02 % aqueous solution of metanil yellow (Sigma–Aldrich)) before aerosol collection. The UV-visible spectrum of metanil yellow in the presence of acidic aerosol was monitored by reflectance UV-visible spectroscopy (Lambda 35 UV WinLab V5.2, PerkinElmer) coupled with an integrating sphere attachment (50-mm integrating Sphere Lambda 2–40). The RH was varied from 20 to 90 % with the aerosol filter sample exposed to the air in a small flow chamber inside of the UV-visible spectrometer. The proton concentration within the aerosol can be measured in terms of the colour change of the indicator on the filter.

(S1)

where A_{545} is the UV absorbance of protonated metanil yellow, which peaks at 545 nm, α is the coefficient of proportionality between the amount of the dye that interacts with acidic aerosols and the mass of inorganic aerosol (M_{inorg}) collected on the filter, m is the unknown constant characteristic of the dye (metanil yellow) in the sulfuric acid system, and $\log_{10} K_a$ is the negative base-ten logarithm of the acid dissociation constant of the dye.

To calibrate the C-RUV technique, different amounts of $NH_4H_3(SO_4)_2$ aerosol and $(NH_4)_7H_{13}(SO_4)_{10}$ aerosol were collected on the filter dyed with metanil yellow. The A_{545} of the aerosol under various RHs was monitored using the C-RUV method. The effect of humidity on the aerosol mass, which is due to the aerosol water content equilibrating with the ambient moisture, was estimated using E-AIM Model II. The proton concentrations of the aerosols used in the calibration were directly predicted using E-AIM Model

II for a given aerosol chemical composition and RH. To obtain the calibration curve with Eqn S1, three parameters (α , m and pK_{BH^+}) were optimised to 28 data points using a solver. The resulting α was 0.105, m was 0.149 and pK_{BH^+} was -1.542 . The proton concentration predicted using E-AIM Model II was plotted v. the calculated proton concentration from Eqn S1 using the C-RUV method in Fig. S1. A good linear fit ($R^2 = 0.83$) was observed between the E-AIM Model II prediction and the C-RUV method.

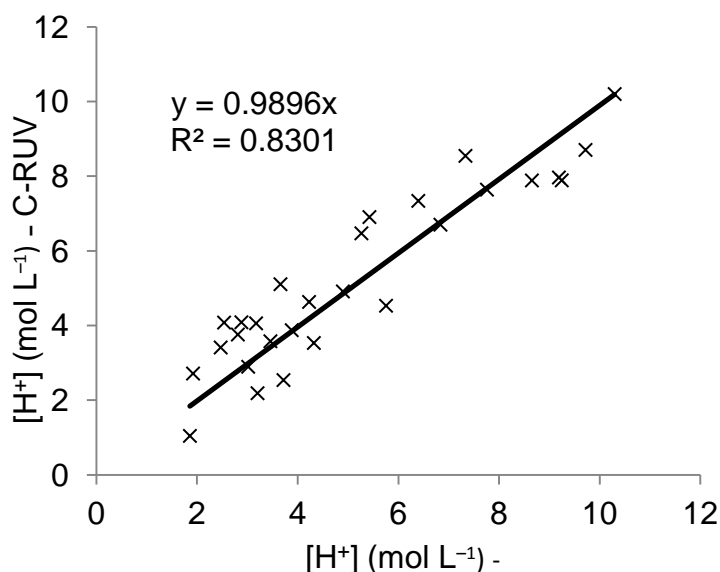


Fig. S1. The correlation of proton concentrations predicted by E-AIM Model II v. that measured using the C-RUV technique.

FTIR setup for aerosol analysis

To experimentally determine the SOA product composition, a Fourier-transform infrared (FTIR) spectrometer (Nicolet Magma 560) equipped with a small flow chamber (0030–104, Thermo Spectra-Tech) that holds an optical window for aerosols collected by impaction (Fig. S2) was used to characterise functional groups of organic compounds in the SOA.^[3,4] The number of FTIR scans is 32 and the wavelength ranged from 400 to 4000 cm^{-1} . The FTIR window was weighed using an analytical balance (MX5 Mettler-Toledo Ltd) before and after particle impaction to measure the mass of the particle sample. The RH inside the flow chamber was controlled by combining humid air from a water bubbler and dry air from an air tank (breathing air, Airgas) with a total air flow rate of 0.6–1.2 L min^{-1} . The RH and temperature of the chamber air were measured with a hygrometer (Dwyer series 485).

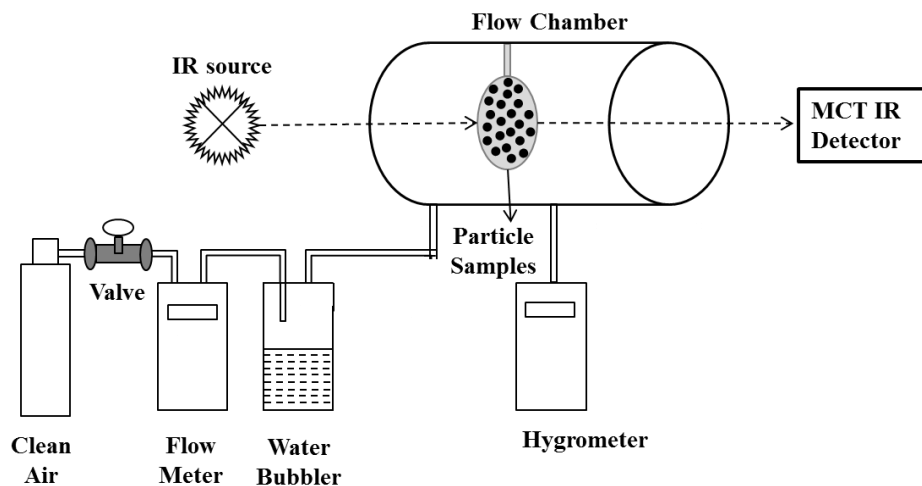


Fig. S2. The experimental set-up for the FTIR studies using a flow chamber.

Analysis of thermodynamically preferred neutral structures in the internally mixed sucrose– NH_4HSO_4 (1 : 3 molar ratio) particle using the FTIR spectrometer

The FTIR spectra of sucrose and diethylsulfate were also recorded to provide references for the FTIR peak assignments (Table S1).

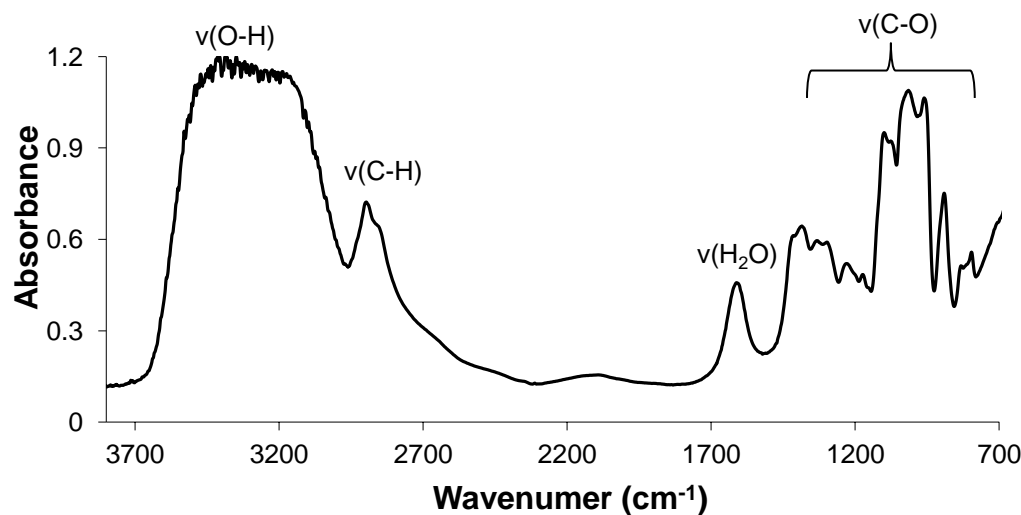


Fig. S3. FTIR spectrum of sucrose on the silicon disc. The number of FTIR scans is 32 and the FTIR wavelength ranged from 400 to 4000 cm^{-1} .

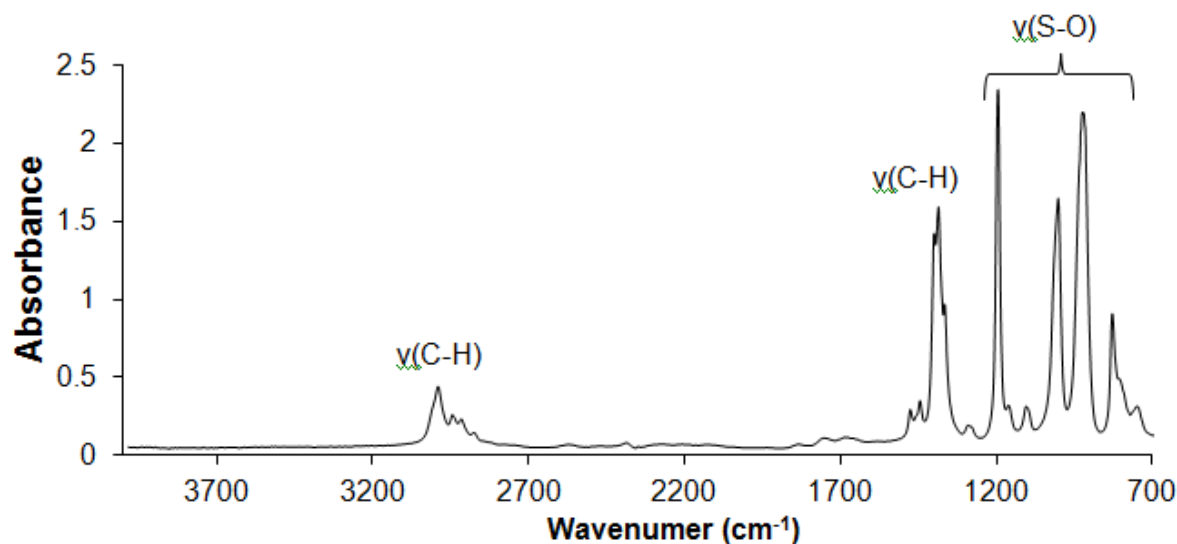


Fig. S4. FTIR spectrum of diethylsulfate on the silicon disc. The number of FTIR scans is 32 and the FTIR wavelength ranged from 400 to 4000 cm⁻¹.

Table S1. FTIR peak assignments of functional groups (underlined) in the internally mixed sucrose–NH₄HSO₄ aerosol

Functional group	FTIR absorbance (cm ⁻¹)	Reference compound
R–C– <u>O–S(O₂)–O</u> –R'	1190, 1000, 827	Diethyl sulfate (Fig. S4), dimethyl sulfate ^[5]
R– <u>O–S(O₂)–O</u> ⁻	1290, 1250, 1080, 1020, 770	Methyl sulfate sodium salt ^[6]
– <u>C–O</u> –	1120, 1040, 922	Sucrose (Fig. S3)
<u>NH₄HSO₄</u>	3220, 3096, 1420	NH ₄ HSO ₄ ^[7]
<u>NH₄HSO₄</u>	1168, 1037, 858	NH ₄ HSO ₄ ^[7]
(<u>NH₄</u>) ₂ SO ₄	3220, 3096, 1420	(NH ₄) ₂ SO ₄ ^[8]
(<u>NH₄</u>) ₂ <u>SO₄</u>	1083	(NH ₄) ₂ SO ₄ ^[5]

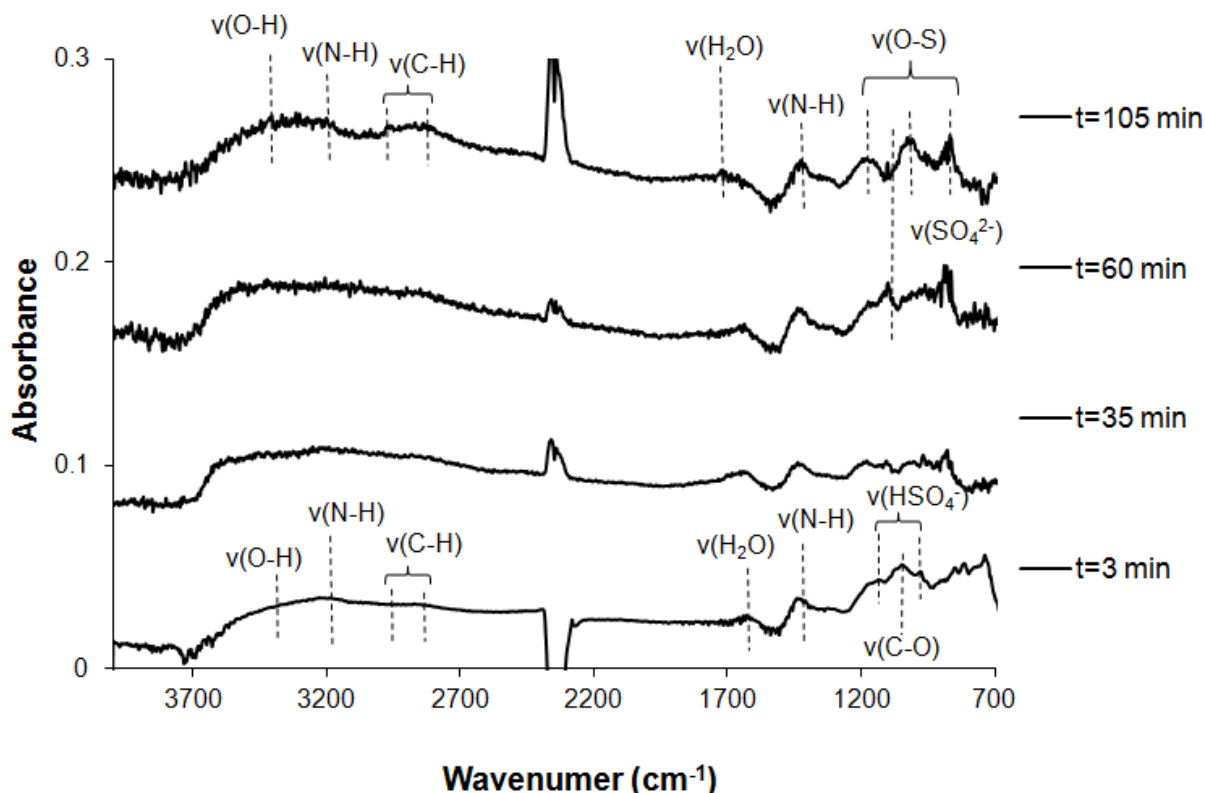
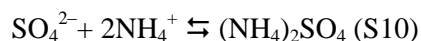
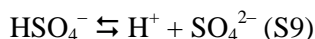
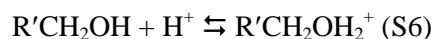
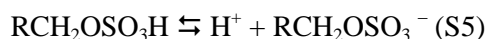
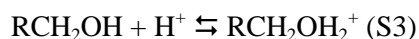
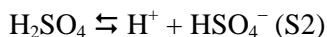


Fig. S5. FTIR spectra of the internally mixed sucrose- NH_4HSO_4 (1 : 3 in mole ratio) aerosol as a function of reaction time.

As shown in Fig S5, the FTIR absorbance spectra of the internally mixed sucrose- NH_4HSO_4 (1:3 mole ratio) aerosol changed over the course of the reaction of sucrose and NH_4HSO_4 . The characteristic bisulfate peaks (1168 and 1037 cm^{-1}) decreased with time, while characteristic peaks associated with the formation of $(\text{NH}_4)_2\text{SO}_4$ (sulfate at 1083 cm^{-1}) and dialkylsulfates (organosulfate peaks at 1190 , 1000 and 827 cm^{-1}) increased. FTIR data suggest that in the ammonium-rich sulfate system, the formation of the mixture of dialkylsulfates and ammonium sulfate is preferred to the formation of ammonium alkylsulfate ($\text{NH}_4\text{SO}_3\text{OR}$, IR peaks at 1290 , 1250 and 770 cm^{-1}). Although FTIR can measure the fractional change in aerosol composition (Fig. S5), FTIR is not an effective method for quantifying the organosulfates. The FTIR peaks of organosulfates overlap with those of inorganic sulfates (Table S1) and other organic compounds at less than 1200 cm^{-1} (Fig. S3).

Mechanisms for organosulfate formation in aerosol

Eqns S2–S11 below describe the reaction mechanisms of the formation of dialkylsulfates by the reactions of acidic sulfate (H_2SO_4 or NH_4HSO_4) with alcohols.



For the reaction mechanisms Eqns S3 to S10, the net reaction is written as:



SOA functional group characterisation using FTIR

To experimentally determine SOA product composition, α -pinene SOA and toluene SOA were collected on the silicon disc and analysed using FTIR (Fig. S2). The FTIR spectra of the SOA samples were decoupled with a curve-fitting method assuming a Gaussian peak. The FTIR peaks used to determine the functional groups are summarised in Table S2.

Table S2. Model organic compounds used for the analysis of the functional group distribution of SOA products using FTIR

The FTIR peak assignments of major functional groups of model compounds are also listed

Compound	Functional group and absorbance wavelength used for FTIR calibration
2-methylprop-1-ene	–C–H (2800–3100 cm^{-1} , 1350–1480 cm^{-1})
<i>n</i> -Pentane	–C–H (2800–3100 cm^{-1} , 1350–1480 cm^{-1})
2-Methyl-1-butene	–C–H (2800–3100 cm^{-1} , 1350–1480 cm^{-1})
<i>n</i> -Hexane	–C–H (2800–3100 cm^{-1} , 1350–1480 cm^{-1})
Propanoic acid	–C–H (2800–3100 cm^{-1} , 1350–1480 cm^{-1}), –COOH (2400–3400 cm^{-1} , 1680–1720 cm^{-1} , 1060–1220 cm^{-1})
Butanoic acid	–C–H (2800–3100 cm^{-1} , 1350–1480 cm^{-1}), –COOH (2400–3400 cm^{-1} , 1680–1720 cm^{-1} , 1060–1220 cm^{-1})
Hexanoic acid	–C–H (2800–3100 cm^{-1} , 1350–1480 cm^{-1}), –COOH (2400–3400 cm^{-1} , 1680–1720 cm^{-1} , 1060–1220 cm^{-1})
Formic acid	–C–H (2800–3100 cm^{-1} , 1350–1480 cm^{-1}), –COOH (2400–3400 cm^{-1} , 1680–1720 cm^{-1} , 1060–1220 cm^{-1})
<i>cis</i> -Pinonic acid	–C–H (2800–3100 cm^{-1} , 1350–1480 cm^{-1}), –COOH (2400–3400 cm^{-1} , 1680–1720 cm^{-1} , 1060–1220 cm^{-1})
Octanoic acid	–C–H (2800–3100 cm^{-1} , 1350–1480 cm^{-1}), –COOH (2400–3400 cm^{-1} , 1680–1720 cm^{-1} , 1060–1220 cm^{-1})
2-Butanone	–C–H (2800–3100 cm^{-1} , 1350–1480 cm^{-1}), –C=O (1680–1720 cm^{-1} , 1060–1220 cm^{-1})
Methylvinylketone	–C–H (2800–3100 cm^{-1} , 1350–1480 cm^{-1}), –C=O (1680–1720 cm^{-1} , 1060–1220 cm^{-1})
4-Ethylcyclohexanone	–C–H (2800–3100 cm^{-1} , 1350–1480 cm^{-1}), –C=O (1680–1720 cm^{-1} , 1060–1220 cm^{-1})
4-Hydroxy-2-butanone	–C–H (2800–3100 cm^{-1} , 1350–1480 cm^{-1}), –C=O (1680–1720 cm^{-1} , 1060–1220 cm^{-1})
2-Hydroxyl-3-pinanone	–C–H (2800–3100 cm^{-1} , 1350–1480 cm^{-1}), –C=O (1680–1720 cm^{-1} , 1060–1220 cm^{-1})
2,5-Hexanedione	–C–H (2800–3100 cm^{-1} , 1350–1480 cm^{-1}), –C=O (1680–1720 cm^{-1} , 1060–1220 cm^{-1})
2,5-Dimethylhexanal	–C–H (2800–3100 cm^{-1} , 1350–1480 cm^{-1}), –C=O (1680–1720 cm^{-1} , 1060–1220 cm^{-1})
Benzaldehyde	–C–H (2800–3100 cm^{-1} , 1350–1480 cm^{-1}), –C=O (1680–1720 cm^{-1} , 1060–1220 cm^{-1})
<i>n</i> -Butanal	–C–H (2800–3100 cm^{-1} , 1350–1480 cm^{-1}), –C=O (1680–1720 cm^{-1} , 1060–1220 cm^{-1})
Octylaldehyde	–C–H (2800–3100 cm^{-1} , 1350–1480 cm^{-1}), –C=O (1680–1720 cm^{-1} , 1060–1220 cm^{-1})
3-Methylbenzyl-alcohol	–C–H (2800–3100 cm^{-1} , 1350–1480 cm^{-1}), –C–OH (3000–3600 cm^{-1} , 1060–1220 cm^{-1})
1-Butanol	–C–H (2800–3100 cm^{-1} , 1350–1480 cm^{-1}), –C–OH (3000–3600 cm^{-1} , 1060–1220 cm^{-1})
4-Hydroxyl-2-butanone	–C–H (2800–3100 cm^{-1} , 1350–1480 cm^{-1}), –C–OH (3000–3600 cm^{-1} , 1060–1220 cm^{-1})
2-Hydroxyl-3-pinanone	–C–H (2800–3100 cm^{-1} , 1350–1480 cm^{-1}), –C–OH (3000–3600 cm^{-1} , 1060–1220 cm^{-1})

Compound	Functional group and absorbance wavelength used for FTIR calibration
1-Octanol	–C–H (2800–3100 cm ⁻¹ , 1350–1480 cm ⁻¹), –C–OH (3000–3600 cm ⁻¹ , 1060–1220 cm ⁻¹)
Sucrose	–C–H (2800–3100 cm ⁻¹ , 1350–1480 cm ⁻¹), –C–O (1060–1220 cm ⁻¹)
Acetic acid butyl ester	–C–H (2800–3100 cm ⁻¹ , 1350–1480 cm ⁻¹), –C–O (1060–1220 cm ⁻¹)
Ethyl acetate	–C–H (2800–3100 cm ⁻¹ , 1350–1480 cm ⁻¹), –C–O (1060–1220 cm ⁻¹)
Ethyl benzoate	–C–H (2800–3100 cm ⁻¹ , 1350–1480 cm ⁻¹), –C–O (1060–1220 cm ⁻¹)
Ammonium sulfate	–N–H (1350–1480 cm ⁻¹ , 3000–3600 cm ⁻¹), –HSO ₄ (1250–1080 cm ⁻¹), H ₂ O (3200–3800 cm ⁻¹ , 1550–1800 cm ⁻¹)
Ammonium nitrate	–N–H (1350–1480 cm ⁻¹ , 3000–3600 cm ⁻¹), H ₂ O (3200–3800 cm ⁻¹ , 1550–1800 cm ⁻¹)
Sodium chloride	H ₂ O (3200–3800 cm ⁻¹ , 1550–1800 cm ⁻¹)

The number of moles of each functional group (n) in the aerosol sample was estimated using the integrated peak area (A) of the decoupled peak of the aerosol sample and that of standard compounds (A_s). The compounds used in the FTIR calibration are listed in Table S2. An aliphatic –C–H stretching band was quantified using the peak at 2800–3100 cm⁻¹.

$$n(\text{–C–H}) = \frac{A}{A_s} \quad (\text{S12})$$

Ammonium was quantified using the N–H absorbance at 1426 cm⁻¹.

$$n(\text{–N–H}) = \frac{A}{A_s} \quad (\text{S13})$$

Then carboxylic acids and alcohols can be quantified.

$$n(\text{–COOH}) = \frac{A}{A_s} \quad (\text{S14})$$

$$n(\text{–C–OH}) = \frac{A}{A_s} \quad (\text{S15})$$

Distinction between aldehydes and ketones was not possible because the weak C–H absorbance of aldehydes (2720–2820 cm⁻¹) could not be observed in any of the SOA spectra. Thus, aldehydes and ketones were quantified as a group (–C=O).

$$n(\text{–C=O}) = \frac{A}{A_s} \quad (\text{S16})$$

The feasibility of the FTIR method was tested for pinic acid, pinonaldehyde and phenol. A good agreement was found between the estimated functional group distribution and the molecular structures of model compounds (Table S3).

Table S3. The relative mole value (normalised by moles of –C–H in each aerosol sample) of functional groups in the model compounds estimated using FTIR analysis v. the actual relative mole value in the compounds

Functional group	Pinic acid		Pinonaldehyde		Phenol	
	FTIR	Real	FTIR	Real	FTIR	Real
–CH–	1	1	1	1	1	1
–C–OH	0		0	0	0.18	0.2
–COOH	0.16	0.17	0	0	0	0
–C=O	0		0.14	0.13	0	0

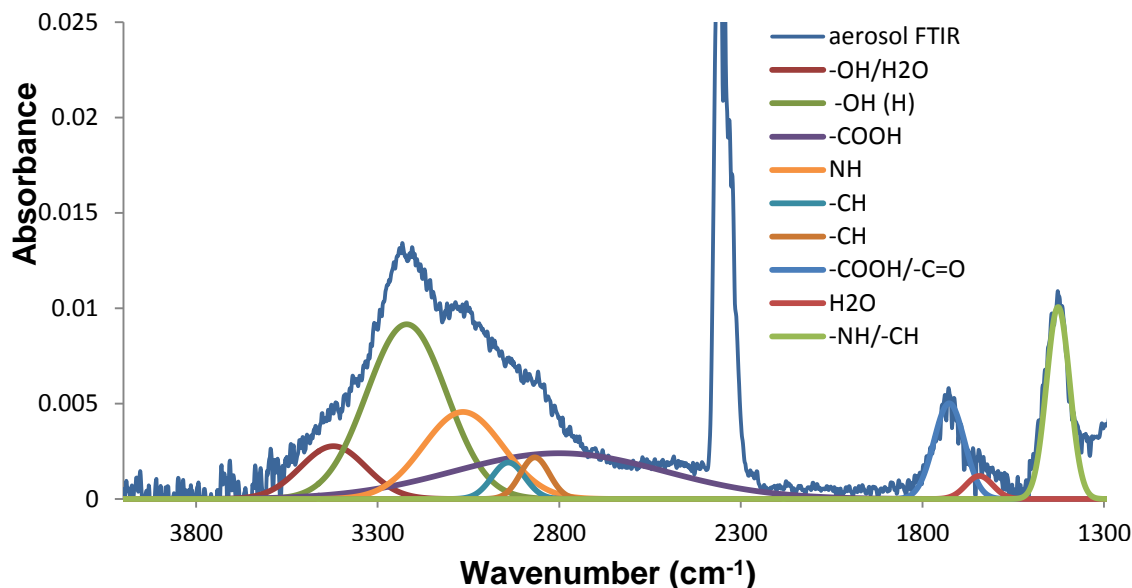


Fig. S6. FTIR spectra of sulfuric acid-seeded α -pinene SOA decoupled into functional groups. Experimental conditions are shown in Set 1 of Table 1 of the manuscript. The number of moles of each functional group in the aerosol sample was estimated using the integrated peak area of the decoupled peak in the aerosol sample and that of standard compounds.

Kinetic simulation of the photooxidation of various VOCs in the presence of NO_x using the UF-APHOR chamber that uses natural sunlight

Isoprene, α -pinene, and toluene were photooxidised in the presence of NO_x with and without sulfuric acid seed aerosol using the UF-APHOR chamber. The simulation of the gas-phase photooxidation in the presence of NO_x was computed using the explicit mechanisms (Master Chemical Mechanism (MCM V3.3)).^[9,10] It is known that the decay of toluene is underestimated in the MCM owing to the low production of OH radicals.^[11] Thus, to fit the simulated toluene decay to the experimentally measured data, an artificial OH radical ($\sim 1.0 \times 10^8 \text{ molecules cm}^3 \text{ s}^{-1}$) was added to the toluene mechanism for the present study.^[12]

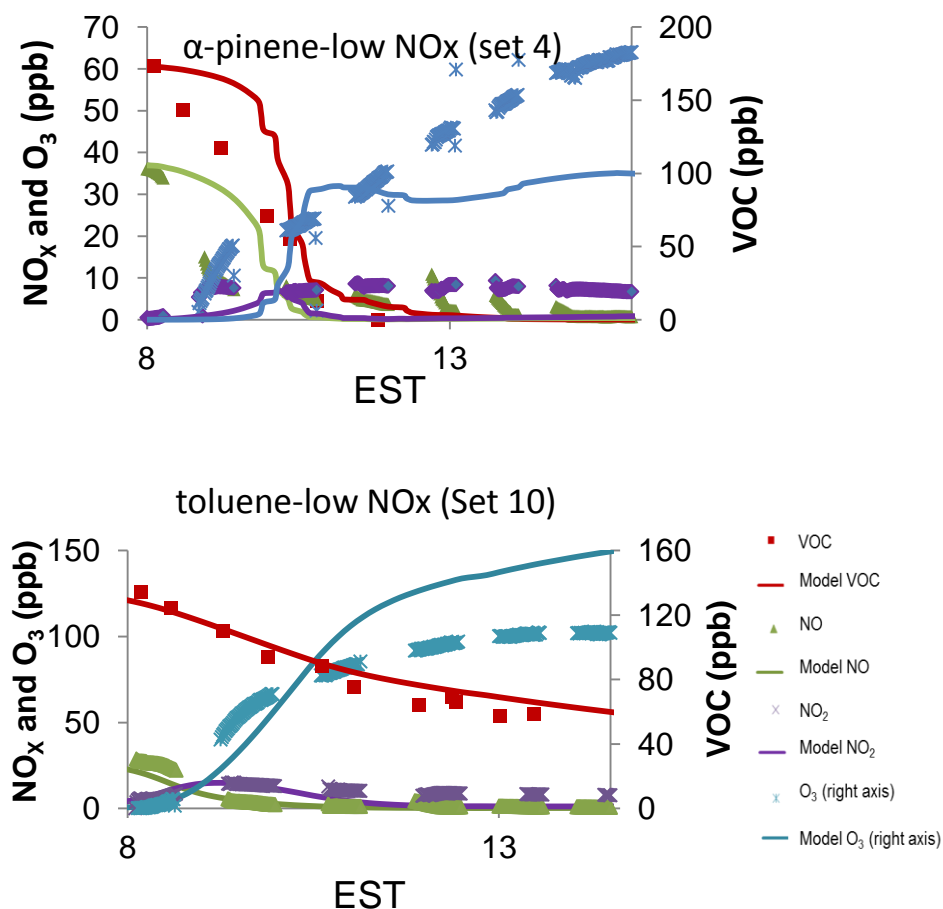
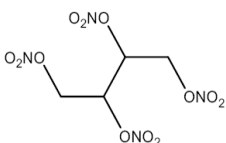
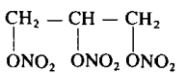
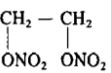


Fig. S7. Time profiles of VOC, NO_x and O₃ predicted using the near-explicit mechanism Master Chemical Mechanism integrated with a kinetic solver and experimental measurements.

Estimation of vapour pressures of organonitrates using group contribution

The vapour pressure of the oxidised products (*i*) were estimated using a group contribution method.^[3] Because there is not a parameter available for the estimating the vapour pressure contribution of organonitrate functional group, the nitrate group was treated as the sum of a nitro group (–NO₂) and an ether (–O–) group. To validate the method to estimate the vapour pressure of organonitrate compounds, the estimated vapour pressures of alklynitrates were compared with literature values (Table S4). The estimated vapour pressures of alkylonitrates agreed well with the literature data for the tested compounds ($R^2 = 0.97$).

Table S4. The estimated vapour pressure of organonitrates treated as the sum of a nitro group (–NO₂) and an ether (–O–) using a group contribution method^[3] v. literature data

Compound	Estimated logP	Literature data logP	Reference
C ₂ H ₅ ONO ₂	1.77	1.81	Goodeve ^[13]
C ₃ H ₇ ONO ₂	1.33	1.26	OSHA/EPA Occupational
C ₄ H ₉ ONO ₂	0.89	0.98	Chemical Database ^[14]
C ₅ H ₁₁ ONO ₂	0.46	0.70	
	–4.73	–4.62	Oxley et al. ^[15]
	–2.72	–2.96	OSHA ^[16]
	–0.42	–1.40	OSHA ^[16]

Estimation of activity coefficients of various organic compounds in salt-containing aqueous solution of aerosol at various RHs

The activity coefficients (γ_{water}) of a compound i in water were estimated under saturated conditions in pure water using Hansen's solubility parameter method,^[17] and the activity coefficients ($\gamma_{\text{in},i}$) of i in the inorganic aqueous phase (with salt) under various RHs were obtained from literature data.^[18–20] For the solubility of organic compounds in an inorganic aerosol, literature solubility data for NaCl aqueous solution were used because of the lack of literature data for SO₄^{2–}–NH₄⁺–H₂O. A multiple linear regression was generated to estimate the relative ratio of γ_{water} to $\gamma_{\text{in},i}$.

$$\text{—} = 0.173 \times \text{RH} + 7.65 \times 10^{-6} \times \gamma_{\text{water}} - 3.18 \times 10^{-4} \text{ (S17)}$$

Fig. S8. The relationship between the activity coefficients (γ_{water}) of organic compounds under saturated condition in pure water and the activity coefficients ($\gamma_{\text{in},i}$) in a salt-containing aqueous phase at varying RHs.

Multiple linear regression to predict dialkylsulfate yields (Y_{diOS–OC–SO₄}) in sulfuric acid-seeded SOA

The functional group concentrations of the SOAs produced under the experimental conditions of the present study (Table 1) were estimated using the thermodynamic model. The resulting concentrations (μmol m^{–3}) of functional groups in the aerosol that interact with the inorganic phase are listed in Table 2. The correlation coefficients between the concentration of each functional group and Y_{diOS–OC–SO₄} were calculated and are shown in Table S5. Strong correlations between the concentration of the alcohol group (–C–OH) and Y_{diOS–OC–SO₄}, and the concentration of the organonitrate group (–ONO₂) and Y_{diOS–OC–SO₄} were observed.

Table S5. Correlation coefficients between organic functional groups and $Y_{\text{diOS-OC-SO}_4}$

Correlation coefficient	–CH–	–COOH	–C–OH	–CHO	–ONO ₂	$Y_{\text{diOS-OC-SO}_4}$
–CH–	1					
–COOH	0.86	1				
–C–OH	0.04	0.52	1			
–CHO	0.71	0.56	–0.07	1		
–ONO ₂	–0.20	0.33	0.90	–0.30	1	
$Y_{\text{diOS-OC-SO}_4}$	–0.52	–0.04	0.76	–0.46	0.88	1

References

- [1] M. Jang, G. Cao, J. Paul, Colorimetric particle acidity analysis of secondary organic aerosol coating on submicron acidic aerosols. *Aerosol Sci. Technol.* **2008**, *42*, 409. doi:10.1080/02786820802154861
- [2] J. Li, M. Jang, Aerosol acidity measurement using colorimetry coupled with a reflectance UV-Visible spectrometer. *Aerosol Sci. Technol.* **2012**, *46*, 833. doi:10.1080/02786826.2012.669873
- [3] M. Jang, R. Kamens, Atmospheric secondary aerosol formation by heterogeneous reactions of aldehydes in the presence of a sulfuric acid aerosol catalyst. *Environ. Sci. Technol.* **2001**, *35*, 4758. doi:10.1021/es010790s
- [4] J. Jang, M. Jang, W. Mui, C. Delcomyn, M. Henley, J. Hearn, Formation of active chlorine oxidants in saline Oxone aerosol. *Aerosol Sci. Technol.* **2010**, *44*, 1018. doi:10.1080/02786826.2010.507612
- [5] *Sulfuric acid, dimethyl ester* **2011** (NIST). Available at <http://webbook.nist.gov/cgi/cbook.cgi?ID=77-78-1> [Verified 2 October 2015].
- [6] *Methyl sulfate sodium salt. CAS Number 512-42-5* **2015** (Sigma–Aldrich Co.) Available at <http://www.sigmaaldrich.com/catalog/product/aldrich/318183?lang=en®ion=US> [Verified 2 October 2015].
- [7] D. J. Cziczo, J. P. D. Abbatt, Infrared observations of the response of NaCl, MgCl₂, NH₄HSO₄, and NH₄NO₃ aerosols to changes in relative humidity from 298 to 238 K. *J. Phys. Chem. A* **2000**, *104*, 2038. doi:10.1021/jp9931408
- [8] *Infrared Spectrum, Ammonium sulfate* **2011** (NIST). Available at <http://webbook.nist.gov/cgi/cbook.cgi?ID=C7783202&Units=CAL&Type=IR-SPEC#IR-SPEC> [Verified 2 October 2015].
- [9] M. E. Jenkin, S. M. Saunders, V. Wagner, M. J. Pilling, Protocol for the development of the Master Chemical Mechanism, MCM v3 (Part B): tropospheric degradation of aromatic volatile organic compounds. *Atmos. Chem. Phys.* **2003**, *3*, 181. doi:10.5194/acp-3-181-2003
- [10] C. Bloss, V. Wagner, M. E. Jenkin, R. Volkamer, W. J. Bloss, J. D. Lee, D. E. Heard, K. Wirtz, M. Martin-Reviejo, G. Rea, J. C. Wenger, M. J. Pilling, Development of a detailed chemical mechanism (MCMv3.1) for the atmospheric oxidation of aromatic hydrocarbons. *Atmos. Chem. Phys.* **2005**, *5*, 641. doi:10.5194/acp-5-641-2005

- [11] V. Wagner, M. E. Jenkin, S. M. Saunders, J. Stanton, K. Wirtz, M. J. Pilling, Modelling of the photooxidation of toluene: conceptual ideas for validating detailed mechanisms. *Atmos. Chem. Phys.* **2003**, *3*, 89. doi:10.5194/acp-3-89-2003
- [12] Y. Im, M. Jang, R. L. Beardsley, Simulation of aromatic SOA formation using the lumping model integrated with explicit gas-phase kinetic mechanisms and aerosol-phase reactions. *Atmos. Chem. Phys. Discuss.* **2013**, *13*, 5843. doi:10.5194/acpd-13-5843-2013
- [13] J. W. Goodeve, The vapour pressures of ethyl nitrate, ethyl nitrite, and nitroethane. *Trans. Faraday Soc.* **1934**, *30*, 501. doi:10.1039/tf9343000501
- [14] *NIOSH Pocket Guide to Chemical Hazards 2015* (Centers for Disease Control and Prevention). Available at <http://www.cdc.gov/niosh/npg/npgd0539.html> [Verified 5 November 2015].
- [15] J. C. Oxley, J. L. Smith, J. E. Brady, A. C. Brown, Erratum: Characterization and analysis of tetranitrate esters. *Propellants Explos. Pyrotech.* **2012**, *37*, 735. doi:10.1002/prop.201280641
- [16] *Ethylene Glycol Dinitrate (EGDN)/Nitroglycerin (NG) 2015* (US Department of Labor). Available at <https://www.osha.gov/dts/sltc/methods/organic/org043/org043.html> [Verified 2 October 2015].
- [17] A. F. M. Barton, *Handbook of Solubility Parameters and Other Cohesion Parameters 1991* (CRC Press: Boston, MA).
- [18] A. Noubigh, A. Mgaidi, M. Abderrabba, E. Provost, W. Fürst, Effect of salts on the solubility of phenolic compounds: experimental measurements and modelling. *J. Sci. Food Agric.* **2007**, *87*, 783. doi:10.1002/jsfa.2762
- [19] C. Bretti, R. M. Cigala, F. Crea, C. Foti, S. Sammartano, Solubility and activity coefficients of acidic and basic non-electrolytes in aqueous salt solutions: 3. Solubility and activity coefficients of adipic and pimelic acids in NaCl(aq), (CH₃)₄NCl(aq) and (C₂H₅)₄NI(aq) at different ionic strengths and at T = 25 °C. *C. Fluid Phase Equilibria* **2008**, *263*, 43. doi:10.1016/j.fluid.2007.09.018
- [20] N. Šegatin, C. Klofutar, Salting-out of some alkyl acetates in aqueous sodium chloride solutions. *Monatsh. Chem.* **2000**, *131*, 0131. doi:10.1007/s007060050014